The Cryosphere Discuss., 6, 849–891, 2012
www.the-cryosphere-discuss.net/6/849/2012/
doi:10.5194/tcd-6-849-2012

The Cryosphere Discussions

Permafrost distribution in the European Alps: calculation and evaluation of an index map and summary statistics

L. Boeckli[1], A. Brenning[2], S. Gruber[1], and J. Noetzli[1]

[1]Department of Geography, University of Zurich, Switzerland
[2]Department of Geography and Environmental Management, University of Waterloo, Ontario, Canada

Received: 7 February 2012 – Accepted: 23 February 2012 – Published: 6 March 2012

Correspondence to: L. Boeckli (lorenz.boeckli@geo.uzh.ch)

Published by Copernicus Publications on behalf of the European Geosciences Union.

Abstract

The objective of this study is the production of an Alpine Permafrost Index Map (APIM) covering the entire European Alps. A unified statistical model that is based on Alpine-wide permafrost observations is used for debris and bedrock surfaces across the entire Alps. The explanatory variables of the model are mean annual air temperatures, potential incoming solar radiation and precipitation. Offset terms were applied to make model predictions for topographic and geomorphic conditions that differ from the terrain features used for model fitting. These offsets are based on literature review and involve some degree of subjective choice during model building. The assessment of the APIM is challenging because limited independent test data are available for comparison and these observations represent point information in a spatially highly variable topography. The APIM provides an index that describes the spatial distribution of permafrost and comes together with an interpretation key that helps to assess map uncertainties and to relate map contents to their actual expression in terrain. The map can be used as a first resource to estimate permafrost conditions at any given location in the European Alps in a variety of contexts such as research and spatial planning.

Results show that Switzerland likely is the country with the largest permafrost area in the Alps, followed by Italy, Austria, France and Germany. Slovenia and Liechtenstein may have marginal permafrost areas. In all countries the permafrost area is expected to be larger than the glacier-covered area.

The permafrost index map with an approximate grid spacing of 30 m is available at the webpage of the Department of Geography, University of Zurich.

1 Introduction

Permafrost in the European Alps is of practical and scientific interest and the regional estimation of its distribution is described in numerous studies (e.g., Hoelzle, 1994; Imhof, 1996; Frauenfelder, 1998; Keller et al., 1998; Gruber and Hoelzle, 2001; Lam-

TCD
6, 849–891, 2012

biel and Reynard, 2001; BAFU, 2005; Bodin, 2007; Ebohon and Schrott, 2008). However, this existing work cannot easily be compiled into an Alpine-wide permafrost map because the relevant studies (a) usually are regionally calibrated, (b) rely on differing methods, and (c) exclude large parts of the Alps. The present study is aimed to overcome these limitations and to provide one coherent Alpine Permafrost Index Map (APIM).

Building upon the formulation of an Alpine-wide permafrost distribution model by Boeckli et al. (2012), the aims of this paper are:

- To create a permafrost map (APIM) displaying index values based on model-derived probabilities of permafrost presence.
- To evaluate the APIM using independent data and discuss the general challenges inherent to this evaluation.
- To develop a legend and interpretation key that allow the efficient use of the APIM as well as an assessment of its most important uncertainties.
- To provide summary statistics regarding permafrost distribution in the Alps.

Based on a systematic collection of permafrost evidence, an Alpine-wide Permafrost MODel (APMOD) has been developed recently (Boeckli et al., 2012). Compared to previous studies, APMOD has unique data basis that is distributed over the entire Alps. However, the difficult challenge that all permafrost distribution models have to deal with is that permafrost as a subsurface phenomenon can not easily be detected at the terrain surface, and direct evidence for its presence or absence is generally rare. Therefore, model development is strongly limited by the type of calibration data available. As a consequence, the derivation of a map-based product from statistical models requires the inference of permafrost conditions in morphological settings other than those used for calibration. This task involves some degree of subjective choice during model application. This paper complements the study of (Boeckli et al., 2012) by describing the required steps towards and the first results of an application of the APMOD.

TCD
6, 849–891, 2012

Regional permafrost distribution models are typically based on empirical-statistical relationships and give indications of permafrost distribution, with limited accuracy demands (Harris et al., 2009). PERMAKART (Keller, 1992) and PERMAMAP (Hoelzle, 1992; Hoelzle et al., 1993) were the first modeling approaches in the Alps that related topographic and climatic variables to the existence of permafrost and that provided map-based products to visualize permafrost distribution. Both models have been applied to various regions and the basic relationships have been used/adapted for the development of further models (Imhof, 1996; BAFU, 2005; Ebohon and Schrott, 2008). As output, both models provide gridded data spatially predicting permafrost occurrence by using discrete classification schemes. While PERMAKART uses the terms "no permafrost", "possible permafrost" and 'likely permafrost", PERMAMAP provides the classes "probable permafrost" and "probable non-permafrost". Other models and classifications use terms like "continuous", "discontinuous", "sporadic" and "isolated" permafrost (Heginbottom, 2002). However, all models have in common that the output of the model consists of classes that are not expressed in measurable ways. This is because the models do not predict probability or extent of permafrost, or ground temperatures but a losely-defined proxy variable.

All discussed modelling strategies, including those proposed in this paper, are not limited to the European Alps but have been developed for and applied to different mountain regions (e.g., Serrano et al., 2001; Tanarro et al., 2001; Janke, 2004; Lewkowicz and Ednie, 2004; Heggem et al., 2005; Etzelmüller et al., 2007; Lewkowicz and Bonnaventure, 2008; Li et al., 2009).

2 Methods

2.1 A permafrost index based on a probability model

The model developed for this study, APMOD is described in detail by Boeckli et al. (2012). It uses mean annual air temperatures (MAAT), potential incoming solar radia-

TCD
6, 849–891, 2012

tion (PISR) and the mean annual sum of precipitation (PRECIP) as explanatory variables and is based on two sub-models for two different land cover classes: The debris model has been calibrated using rock glacier inventories and predicts the probability of rock glaciers being intact as opposed to relict. The rock model is based on mean annual rock surface temperatures (MARST) and predicts the probability of finding MARST $\leq 0\,^{\circ}\mathrm{C}$ in steep bedrock. Both models are combined based on fuzzy membership (linear function depending on slope angle, Sect. 3.2) to the land cover types rock and debris, and allow the inclusion of temperature offset terms. These offset terms are required to generalize APMOD to other surface characteristics than those used for model calibration. When applied to digital elevation models (DEMs) of differing resolution, scaling functions improve the coherence and comparability of the results.

The probabilities of permafrost occurrence derived from APMOD are translated to permafrost index values because the term "probability" is misleading and does not communicate the uncertainties and assumptions that are integrated in our final map-based product: The calibration of APMOD was not possible for many surface types, because permafrost observations are not available in sufficient quality and quantity. To derive a map-based product, we need to infer conditions where we have no data and the uncertainty of such predictions is difficult to assess. The term permafrost index thus avoids the notion of probability as we introduce some estimated additional factors (temperature offsets) and cannot evaluate true probability or extent. We suggest that the index represents an indicator of the probability for permafrost occurrence, the spatial percentage of permafrost per cell and/or the thickness of the permafrost body. The index can also be interpreted as an approximation of the mean annual ground temperature. However, permafrost extent, thickness or temperature cannot be allocated directly with the values of the index, because various local and regional processes are neglected or only approximated by the model.

TCD
6, 849–891, 2012

2.2 Evaluation of a permafrost index map

The evaluation data (Sect. 3.3) is based on rock glaciers and point observations of permafrost presence and absence. Status information (intact vs. relict) of rock glaciers can be used to evaluate the output of APMOD in areas covered by rock glaciers. The point observations allow to evaluate the map for other types of surfaces but these main challenges exist: (a) The number of observations is very small compared to the study area and the observations are strongly biased towards permafrost existence; (b) Even less evidence in steep bedrock as well as in intermediate slopes between debris cover and steep bedrock is available; (c) When combing data of different research groups, based on different techniques and coordinate systems, the quality and consistency of the data is a major challenge and errors (e.g., shift in coordinates) can not be excluded; (d) While the output of APMOD is grid-based with cells having an area of approximately 900 m^2, the observations represent point information within a complex, spatially variable mountain topography. This problem relates to sub-grid variability and scaling issues (cf. Gubler et al., 2011).

To address point (c) and (d) an additional measure describing the agreement of the terrain attributes (PF_{loc}) was calculated for each observation point: The terrain variables elevation, slope angle and aspect were derived from the digital elevation model ASTER GDEM (Hayakawa et al., 2008) for all 352 observation points and then compared to the values that were manually entered by the data provider into the permafrost evidence data base. It is not possible to automatically differentiate errors in the evidence metadata from the effects of sub-grid variability with this method. It is, however, useful to have this index of topographical agreement for the interpretations of differences in the comparison and for further investigating possible errors in the evidence data. Differences in aspect values (Δ_A) were calculated using the absolute difference between aspect angles modulo 360° in the interval [−180°, 180°]. Thresholds were then manually chosen to weight these differences and to derive PF_{loc} (Sect. 3.3).

TCD
6, 849–891, 2012

To assess the discrimination of the permafrost index the area under the receiver-operating characteristics curve (AUROC, Mason and Graham, 2002) was measured. This measure ranges from 0.5 (random discrimination) and 1 (perfect discrimination).

2.3 Calculation of summary statistics

The term "permafrost index area" will be used to present the result and refers to the area having an index equal or higher than a specified threshold. Glaciers are excluded from the permafrost index areas. It is important to note the difference to permafrost area that would be defined as the surface actually underlain by permafrost (cf. Zhang et al., 2000; Gruber, 2012). The index area is the unit of interest for decision-making ("Where do I need to consider permafrost?") and the actual result of the model presented. Permafrost area may be important for, e.g., estimating water storage, but is more difficult to support by reliable data.

Pixel area of the unprojected ASTER GDEM grid depends on latitude (ϕ) and the mean radius of the Earth (R = 6371 km). North-South (Δy) and West-East (Δx) for the $1''$ spherical grid were used to calculate the area:

$$\Delta y = \frac{\pi R}{21600} \text{ and } \Delta x = \cos(\phi)\Delta y \quad (1)$$

The software R (version 2.14.1; R Development Core Team, 2010) was used for all statistical analyses. Terrain and geodata analyses were conducted with "RSAGA" (Brenning, 2008) and "raster" (Hijmans and van Etten, 2012) packages for R.

3 Data

3.1 Topography and climate

The topographic and climatic variables were calculated according to Boeckli et al. (2012) with Alpine-wide datasets: PISR estimates were computed based on ASTER

TCD
6, 849–891, 2012

GDEM. Alpine-wide MAAT data for the period 1961–1990 (Hiebl et al., 2009), which is based on the GTOPO30 elevation model (Center, 1997) was adjusted with more precise elevation information of the ASTER GDEM using a constant lapse rate of 0.0065 °C m^{-1} (cf. International Organization for Standardization, 1975). Slope angles to differentiate rock and debris cover were derived from the ASTER GDEM using the algorithm of Travis et al. (1975), which calculates the maximum slope in a 3×3 window. PRECIP was computed for the period 1961–1990 using monthly precipitation data (gridded at 10′ spatial resolution, approximately 15 km, Efthymiadis et al., 2006).

3.2 Surface types

A land cover map defining the two surface types (debris cover and steep bedrock) for the application of the two sub-models is required for APMOD. A transition zone with varying degree of membership for the two surface types is used where APMOD is applied using a combination of the two sub-models (debris and rock model). In this paper, additional surface types are introduced as a spatial basis for addressing the offsets and assumptions described in Sect. 4. The following land surface types are differentiated and described below: debris cover, steep bedrock, vegetation and glacier coverage.

Steep bedrock and debris cover: The distinction between these two model domains is based on slope angle alone: We define an index m_r by

$$m_r' = \frac{S - S_{\min}}{S_{\max} - S_{\min}}, \tag{2}$$

$$m_r = \begin{cases} 0 & \text{if } m_r' \le 0 \\ 1 & \text{if } m_r' \ge 1 \\ m_r' & \text{otherwise,} \end{cases}$$

which describes the degree of membership in the steep bedrock surface class, where S is the slope angle of the grid cell, $S_{\min}$ is a fixed threshold angle up to which only

TCD
6, 849–891, 2012

debris cover occurs, and S_{max} is the assumed maximum slope angle up to which the surface may be debris-covered. In agreement with Boeckli et al. (2012) the term "steep bedrock" is defined as terrain that (a) is not or only marginally affected by a snow cover in wintertime, (b) does not contain large amounts of blocks and/or debris, and (c) is without vegetation coverage. Based on a literature review, Pogliotti (2010) summarizes that slope angles of 35–37 represent the upper limit of usually well snow-covered areas (S_{min}) and slope angles of 55–60 define the upper limit of snow accumulation (S_{max}). Analyzing the distribution of slope angle values within training areas representing debris respectively bedrock cover (Fig. 1) indicates similar values for the two thresholds based on the data used here. The training areas were derived from the land cover map of Switzerland (Vector25, swisstopo, 2007) using randomly distributed points (N = 4029 for rock and N = 4381 for debris cover). Here, the distribution of slope angle values is biased because bedrock is also possible in flat terrain (e.g. glacier forefields) and the number of points that are used for this analysis are sparse for very steep slopes.

Finally, S_{min} was set to 35°, which coincides with the start of a strong increase in the presence of exposed bedrock (Fig. 1) and S_{max} was set to 55°. Slopes with greater slope angles in the DEM rarely present debris surfaces (Fig. 1), and these can likely be attributed to errors in the DEM. To address point (c), we assume a debris cover (m_r = 0) if the surface is covered by vegetation (see below).

Vegetation: The discrimination of vegetation from vegetation-free surfaced areas is based on the soil-adjusted vegetation index (SAVI; Huete, 1988) and is derived from Landsat Thematic Mapper (Landsat 5) and Landsat Enhanced Thematic Mapper (Landsat 7) images using red and near-infrared (NIR) wavelengths. SAVI accounts for the soil-induced influences on vegetation index values and involves an additional constant L to the formula of the normalized difference vegetation index (NDVI):

$$SAVI = \frac{\text{NIR} - \text{red}}{\text{NIR} + \text{red} + \text{L}}(1 + L) \quad (3)$$

TCD
6, 849–891, 2012

L was set to 1, since this value is suitable for characterizing low vegetation densities (Huete, 1988) present in mountainous vegetation. 13 scenes cover the entire Alpine region. Only images taken in August/September/October were used, since vegetation is still well-developed as evidenced by remotely sensed phenology (cf. Fontana et al., 2008) and snow cover is likely near its annual minimum. For each of the 13 scene locations, the scene with lowest cloud cover was chosen (Table 1). After calculating the SAVI values, all 13 grids were merged and resampled with bilinear interpolation to the resolution of ASTER GDEM.

A threshold for discriminating vegetation from vegetation-free surfaced areas was chosen by analyzing SAVI values in training areas derived from Vector 25. The training data consists of randomly distributed points: 42,797 for vegetation and 8419 for vegetation free areas. The Vector 25 land cover classes "rock" and "debris"; were treated as vegetation-free areas, while "forest", "open forest", "bush land" and "remaining areas" were classified as vegetation. Finally, optimizing the κ coefficient (Cohen, 1960) as a function of the SAVI threshold, pixels with $SAVI < 0.335$ are considered free of vegetation and pixels with SAVI$\geq$ 0.335 are classified as vegetation. Further a median filter (3x3 cells) was applied to remove artefacts, and all pixels where $m_r = 1$ (steep bedrock) were considered free of vegetation.

Glaciers: Glacier outlines derived from Landsat images were provided by Paul et al. (2011). The outlines represent glacier extent in the year 2003, manually corrected for debris-covered glacier parts.

3.3 Evaluation data

As a result of matched sampling, Boeckli et al. (2012) excluded 394 intact and 2403 relict rock glaciers from model fitting, which are available for model evaluation in the debris cover domain (Fig. 2).

Additional 352 point observations are available within the permafrost evidence collection (Fig. 2; Cremonese et al., 2011) that were not used for model calibration. These observations are based on different methods and were classified as permafrost pres-

TCD
6, 849–891, 2012

ence or absence by each individual data contributor. This classification was also rated by the data contributor with an index that describes the certainty of this classification (PF_{cert}).

As described in Sect. 2.2, a second measure describing the agreement of terrain attributes (PF_{loc}) was introduced. Absolute differences in elevation, slope and aspect angle (Fig. 3) were used to manually define thresholds and to weight these differences (Table 2). The weight of the variable aspect was disregarded for slope angles $\leq 15^{\circ}$, because uncertainties in this variable are large for flat terrain. Multiplying the assigned weights for the three measures elevation, slope angle and aspect for each observation results in values ranging from 0 to 8, where a value >= 4 is classified as "agree", a value of 1–2 "disagree" and a value of 0 "strongly disagree" (Table 3). The multiplication of the three weights implies that an observation with one of the three measures = 0 is classified as "strongly disagree" whatever the other two measures are.

4 Estimation of offset terms

In this section, temperature offsets (cf. Sects. 3.1 and 3.2 in Boeckli et al., 2012) for the surface types rock, debris and vegetation are defined, which are applied to APMOD to obtain a map product resulting in APIM. An overview of the discussed offset terms is given in Table 4.

The MARST used for model calibration were measured in homogenous rock following the procedure outlined in Gruber et al. (2003). This provides a quantification of the influence of topography on rock temperatures, but likely, temperatures at greater depth in most rock faces are lower due to effects of snow, debris and fracturing (Gruber and Haeberli, 2007): Measurements in the Swiss Alps showed that the spatial variation of temperature offset in rock faces is large, mainly depending on (a) radiation exposure (Hasler et al., 2011), (b) snow depth and its timing (cf. Pogliotti, 2010) and (c) the amount and characteristics of cleft systems at the rock surface (Hasler et al., 2011). Summarizing these three factors, Hasler et al. (2011) postulate that radiation-exposed

TCD
6, 849–891, 2012

steep rock faces with interspersed snow patches and/or large fractures are up to 3 °C colder at depth (i.e. in the order of a few meters) compared to MARST in snow-free and compact rock. In north-exposed situations the effect of snow and/or fractures is less important, because radiative heat transfer is less dominant. Based on these findings, the offset term Δ_R was implemented as a linear function of PISR and applied to the rock model:

$$\Delta_R = O_{min} + PISR \frac{O_{max} - O_{min}}{350\ W\,m^{-2}}, \quad (4)$$

where O_{min} is the minimal and O_{max} is the maximal offset for pixels where PISR= 350 W m^{-2}. (The percentile of 350 W m^{-2} is 0.88 in the cumulative distribution function of PISR values.) O_{min} was set to −0.5 and O_{max} = −2.5. Spatial variation of Δ_R and offsets depending on other variables (e.g. thermal conductivity) are not considered.

The debris model provides an optimistic estimate (biased towards an overestimation) of permafrost occurrence in debris surfaces because of three main rock glacier characteristics: (a) cooling effect of coarse block surface (e.g. Haeberli et al., 2006), (b) rock glacier movement towards lower elevations (e.g. Barsch, 1978), and (c) delayed response of ice-rich permafrost to climatic forcing (e.g. Frauenfelder et al., 2008). Consequently, it is desirable to find relationships to infer conditions below surfaces other than rock glaciers. The first two sources of bias are considered in this study, while the third remains unaccounted for due to a lack of information that would allow its estimation.

By moving down-slope, a rock glacier transports a cold and ice-rich mass from its rooting zone to conditions that may be less favourable for the formation of permafrost. The melting of ice as a result of an increase in active layer thickness can thus exert a cooling influence on ground temperatures at depth and preserve permafrost where it would not form without the advection of ice-rich material. We approximate the magnitude of this effect by the altitudinal extent of rock glaciers i.e., the difference in elevation between the lowest and highest point of each rock glacier, assuming that in the Alps,

TCD
6, 849–891, 2012

only the rooting zone of a rock glacier shows conditions for the development of ice-rich permafrost. For the 5541 rock glaciers in the inventory of Cremonese et al. (2011), the mean altitudinal extent is 139 m. In APMOD, a random point within each rock glacier is taken for model calibration (Boeckli et al., 2012), which, on average, corresponds to the centroid of the rock glacier. Accordingly, the altitudinal extent is divided by two resulting in a bias correction of 70 m, which corresponds to an approximate difference in MAAT of 0.5 °C (assumed lapse rate 0.0065 °C m^{-1}). This value is chosen for the movement-related offset (Δ_{Da}) and applied to the debris model.

A surface cover of coarse blocks with no or little infill by fine material usually results in markedly colder MAGT than e.g., fine moraine-derived soil or solid bedrock. This effect has been measured and discussed by several researchers (e.g., Humlum, 1997; Harris and Pedersen, 1998; Gorbunov et al., 2004; Hanson and Hoelzle, 2005; Gruber and Hoelzle, 2008; Gubler et al., 2011). Ground temperatures of coarse blocks in comparison to finer grained material may be 1.3–2 °C (Juliussen and Humlum, 2008) to 4–7 °C (Harris and Pedersen, 1998) colder. 1.6 °C to 2.2 °C reduction of MAGT with respect to finer grained material was observed during one year at Corvatsch (Switzerland) for a large data set containing 390 temperature sensors distributed in 39 footprints (Gubler et al., 2011). Accordingly, an offset of 2 °C (Δ_{Db}) is implemented in the debris model to address the effect of coarse blocks. While Δ_{Da} is applied to the whole domain of the debris model, Δ_{Db} is applied to vegetated areas only (see below), because these areas are normally characterized by fine grained debris and can be detected by remote sensing for the entire Alps.

Several studies indicate that in the European Alps, a closed vegetation cover usually indicates the absence of permafrost (Haeberli, 1975; Hoelzle et al., 1993). However, this relationship is not necessarily true in all situations (e.g. Delaloye et al., 2003), but provides a valuable indication. In the context of APIM, we regard a closed vegetation cover to be indicative of fine material and thus the absence of open-work block cover. Therefore the above-mentioned offset (Δ_{Db}) addressing coarse blocks is applied to account for thermal differences between non-vegetated and vegetated areas.

TCD
6, 849–891, 2012

5 Interpretation key for the permafrost index

A sample map of APIM is shown for the Rimpfischhorn in Switzerland (Fig. 4). The map should be used with the provided legend and interpretation key (Fig. A1). An additional map showing the surface types (Fig. 5) is necessary in order to reproduce the statistical model and to interpret the shown index value more accurately.

The aim of the interpretation key provided with the permafrost index map is to allow efficient use and understanding of the map and to communicate the most important uncertainties for practical use by, e.g., public authorities or for infrastructure planning and maintenance. It consists of three parts, (a) the legend itself and an accompanying text, (b) an interpretation key that allows to refine the estimate shown in the map based on additional surface cover observations, and (c) a description and a legend explaining the auxiliary surface-cover map provided (Appendix A1). The index varies from 'permafrost in nearly all conditions' to 'permafrost only in very cold conditions' and describes semi-quantitatively the occurrence of permafrost. The two terms communicate to some degree an uncertainty in the map, and they consequently allow for further interpretations.

A different map signature is used for glaciers, which are by definition not permafrost, although cold glaciers can have permafrost conditions at their bed (e.g., Haeberli and Funk, 1991; Vincent et al., 2007) and the development of permafrost after the disappearance of temperate glaciers is possible (Kneisel et al., 2000).

The accompanying text describes the most important limitations of the map and explains the usage of the interpretation key. Based on the pictures and the text of the interpretation key, the map user should be able to understand and apply this additional information. A "call for feedback" was sent to several permafrost researchers in Europe. Seven replies helped improve the legend and interpretation key.

TCD
6, 849–891, 2012

6 Evaluation of the permafrost index map

The aim of this subsection is to communicate a semi-quantitative assessment of APIM. Comparing the final map index with the distribution of intact and relict rock glaciers shows the model performance in debris-covered areas (Fig. 6). 1863 of the 2403 relict rock glaciers and 42 of the 395 intact rock glaciers show no index value and permafrost is expected to be absent. The majority (68 %) of the remaining 540 relict rock glaciers lies within a permafrost index < 0.4, whereas most (63 %) of the remaining 353 intact rock glaciers are located in areas with an index > 0.5 (mean index equals 0.58). The discrimination of rock glacier status based on predicted permafrost index values results in an AUROC of 0.78 that is an acceptable value according to Hosmer and Lemeshow (2000).

From the permafrost point-observations (Table 3), observations with PF_{loc} equals 'strongly disagree' and PF_{cert} equals "quite likely" are not considered for model evaluation. The predicted permafrost index values for borehole temperatures, geophysical investigations and trench or construction sites cover the entire range from 0 to 1 for permafrost-existence observations (Fig. 7) with mean index values of: 0.80 (borehole temperatures), 0.32 (geophysical investigations) and 0.38 (trench or construction sites). The index values of the permafrost-absence observations range from 0 to 0.44, except one construction site. The discrimination for these tree observations types shows an AUROC = 0.6. When neglecting the offset terms discussed in Sect. 4, the AUROC results in 0.56. If the offset term Δ_{Db} is applied based on local terrain and vegetation information provided by Cremonese et al. (2011) instead of vegetation information derived from SAVI, the AUROC results in 0.67.

The following evidence types from Table 3) were not considered for model evaluation: (a) Ground surface temperatures were not considered because of the large interannual variability caused by the strong influence of the snow cover (Hoelzle et al., 2003; Brenning et al., 2005), (b) Rock fall scars were excluded because only 4 observations remained after removing observations with PF_{loc} equals "strongly disagree", (c) Sur-

TCD
6, 849–891, 2012

face movements were not considered because only 4 observations are available, and d) Other indirect evidence were excluded because no additional information regarding measurement or observation type are available.

7 Calculation of summary statistics

The area potentially influenced by permafrost in the Alps (43° – 49° N, 4° – 16° E) ranges from 2000–12 000 km^2 (Table 5) and the meaning of this range will be discussed in Sect. 8. The largest extent of permafrost is between 2600 and 3000 m depending on the index chosen as threshold, whereas the largest area of glaciers is located above 3000 m (Fig. 8). The offset Δ_{Db} that is applied to the debris model for all vegetated pixels plays an important role regarding the final output map or summary statistic. Neglecting Δ_{Db} increases the potential permafrost area in the entire Alps by approximately 20 %, respectively 3147 km^2 (calculated for an index ≥ 0.1, Table 6).

According to this analysis, Switzerland is the country that contains the largest permafrost area (Table 7). In Italy and Austria also large permafrost areas exist.

8 Discussion

8.1 Interpretation of permafrost index area

The comparison of permafrost index areas obtained in this study with estimates from the literature is complicated by differences in terminology and methods used. Considering index values ≥ 0.5 is one possible assumption to estimate the area affected by permafrost (see Table 7). For Switzerland, the estimated permafrost area then results in 2163 km^2. For comparison, Keller et al. (1998) estimated the permafrost area in Switzerland to range from 4–6 %, which corresponds to approximate 1651–2477 km^2. In Austria, 1600 km^2 were assigned to mountain permafrost by Ebohon and Schrott

TCD
6, 849–891, 2012

(2008) whereas our estimate is 1557 km^2. For France, a value of 1200 km^2 is published (PERMAFRANCE, 2010), which does not correspond well with our estimate (703 km^2).

While these results are encouraging, all estimates are subject to large uncertainties and face the problem of differing or missing definitions for "permafrost area".

8.2 Evaluation of APMOD

The evaluation of APMOD shows that the prediction of the model is reasonable for rock glaciers and boreholes. For "trench or construction sites" as well as for "geophysical investigations" the predicted permafrost index values are in general too low for permafrost presence, but the discrimination of permafrost absence and presence is correct. All three observation types show low index values for permafrost presence, which means that permafrost is also possible at low index values. Partly, this distribution of index values can be explained by the bias towards permafrost existence observations (mean index value of all observations from Fig. 7 = 0.35) induced by the tendency of permafrost researchers to choose locations that do have permafrost. The discrimination of the model is slightly worse when the offset terms are not included, which supports our chosen strategy to include them. Further, the model performance increases, when introducing local terrain and vegetation information to apply the offset terms. This highlights the importance of small-scale heterogeneity and the potential to improve the model's prediction by using the interpretation key and site observations.

8.3 Uncertainties and limitations of APMOD

Temperature offsets used in this study are based on a qualitative assessment of recent literature and on the assumption of remaining constant across the study region. We consider these assumptions and estimates to be the best possible guess given the information available at this time.

The radiation dependent offset (Δ_R) that is included in the rock model ranges from −0.5 °C (minimal PISR) to −2.84°C(maximal PISR) which corresponds to an altitudinal

TCD
6, 849–891, 2012

shift of 77–437 m (assumed lapse rate of 0.0065 °C m^{-1}). Minimal and maximal offset terms are based on investigations by Hasler et al. (2011), but the dependencies based on radiation represents a strong simplification because no information of the surface and subsurface characteristics is available here. Therefore, the maximal uncertainty of the offset within the rock model is derived from the difference between minimal and maximal offset terms and is estimated to be 2.34 °C (e.g., an altitudinal shift of the lower permafrost limit of ±360 m).

The movement-related offset within the debris model is +0.5 °C, respectively 70 m, and is based on the mean altitudinal extent of the analyzed rock glaciers. The standard error of this mean value is given by the standard deviation of the sample (81 m) divided by the square root of its quantity (N = 5541) and results in 1.1 m. However, local variability of rock glacier extent is not accounted for with this movement-related offset.

The effect of coarse blocks is addressed in the debris model with an offset of 2 °C. Here, we assume that the surface characteristics of rock glaciers are constant and we neglect the fact that rock glaciers with fine-grained material also exist in the Alps (e.g., Matsuoka et al., 2005). As discussed in Sect. 4, values from literature for this cooling effect range from 1.3 °C (Juliussen and Humlum, 2008) to 7 °C (Harris and Pedersen, 1998). Thus, we assume this temperature offset to vary between −0.7 °C and +5 °C, corresponding to an altitudinal variation of the order of −153 to +770 m.

The discussed uncertainties in the offset terms are large and influence the final permafrost distribution on the map. However, the interpretation key allows the map user to capture some of these extreme topographical situations and to refine the estimate of the map.

The classification of the surface types as described in Sect. 3.2 is based on simple approaches, and we distinguish between rock, debris, vegetation and glacier cover. Especially the former two surface types are often hard to differentiate and all kind of mixture forms exist in reality. The chosen approach allows classifying these surface types Alpine-wide. For local model application, a more accurate land surface map could be used instead.

TCD
6, 849–891, 2012

APMOD does not account for the recent warming in air temperatures due to climate change and represents a static snapshot of potential permafrost distribution. This is justified because the deviation of an updated and transient permafrost distribution would require knowledge of subsurface ice content that can preserve permafrost conditions for decades. For the purposes of this map ("Where do I need to consider permafrost?") a steady-state distribution is therefore sufficient and will likely remain relevant in the coming decades.

The rock model was adjusted with longer-term mean annual air temperatures for the period 1961–1990 and predicted MARST values correspond to the same period. Rock wall temperatures react rapidly to climate change (Gruber and Haeberli, 2007), whereas rock glaciers response delayed to air temperatures due to high ice content (e.g., Haeberli et al., 2006) and coarse blocky surface. Additionally, transient effects, as well as three-dimensional topographical effects can be responsible for colder temperatures at larger depth than expected based on today's climate conditions (Noetzli and Gruber, 2009). In the final map (APIM) glacier outlines from the year 2003 were used. Because glaciers are subject to fast changes, recently de-glaciated areas need be assessed with caution (e.g., Kneisel, 2004; Kneisel and Kääb, 2007).

9 Conclusions

The statistical model of Boeckli et al. (2012) was used to estimate the current permafrost distribution in the European Alps. This is the first uniform modelling approach that includes all Alpine countries. The Alpine Permafrost Index Map (APIM) uses a grid spacing of approximately 30 m and offers an index ranging from 0 to 1. A high index value point to permafrost in nearly all conditions and a low index value means permafrost only in very cold conditions. Together with the legend and interpretation key this product should be useful for both researchers and stakeholders to estimate the permafrost distribution for a given region in the European Alps. The main conclusions are:

TCD
6, 849–891, 2012

– The transition of a statistical permafrost distribution model to a permafrost map requires a generalization of the model to other surface types than used for model calibration. Therefore additional offset terms were defined qualitatively based on the literature; however, they involve some degree of subjectivity.

– Evaluation of spatially distributed models predicting permafrost is challenging because test data is limited and its distribution biased towards permafrost presence. For future model calibration and evaluation ground truth data needs to be collected using a suitable sampling design in order to avoid site selection bias inherent in convenience sampling.

– Calculated permafrost index areas provide an indication of possible permafrost extents in different subregions of the Alps. The relative area of permafrost occurrence in the Alps is estimated to vary between 1% and 6%. However, it is not possible to calculate exact permafrost extents because we introduced estimated additional offsets.

Possible next steps are the evaluation of the statistical model APMOD with process-based models and the extension of the modelling approach to other mountain regions.

10 Data availability

The APIM is freely available as a kmz overlay for Google Earth and as a Web Mapping Service for use in a GIS environment (accessible at: http://www.geo.uzh.ch/microsite/cryodata/PF_map_explanation.html). The map and interpretation key can be downloaded as an image file. Additionally, a land-cover map (cf. Fig. 5) that defines the used vegetation mask as well as the distinction of debris cover and bedrock based on slope angle is available.

TCD
6, 849–891, 2012

Acknowledgements. Funding of this study was partly provided by the Alpine Space Program project PermaNET, the Bavarian Environment Agency (Bayerisches Landesamt für Umwelt, LfU), the Swiss Federal Office for the Environment (Bundesamt für Umwelt, BAFU), the Autonomous Province of Bolzano and the Region of Veneto, Geological Survey. The precipitation data was provided by the ALP-IMP project http://www.cru.uea.ac.uk/cru/data/alpine/. Landsat scenes are available online (GLOVIS, http://glovis.usgs.gov). Vector25 was provided by the Federal Office of Topography, swisstopo. We thank Wilfried Haeberli for his input on a previous version of this manuscript. Constructive comments on the interpretation key by several colleagues are gratefully acknowledged.

References

BAFU: Hinweiskarte der potentiellen Permafrostverbreitung in der Schweiz, Swiss Federal Office for the Environment (FOEN), 2005. 851, 852

Barsch, D.: Active rock glaciers as indicators for discontinuous alpine permafrost. An example from the Swiss Alps, in: Proceedings of the 3th International Conference on Permafrost. Edmonton, Canada, 10–13 July, 1, 349–352, 1978. 860

Bodin, X.: Géodynamique du Pergélisol Alpin: Fonctionnement, distribution tt évolution récente. L'Exemple du Massif du Combeynot (Hautes Alpe), Ph.D. thesis, Université Denis Diderot Paris 7, France, 2007. 851

Boeckli, L., Brenning, A., Gruber, S., and Noetzli, J.: A statistical approach to modelling permafrost distribution in the European Alps or similar mountain ranges, The Cryosphere, 6, 125–140, doi:10.5194/tc-6-125-2012, 2012. 851, 852, 855, 857, 858, 859, 861, 867, 884

Brenning, A.: Statistical geocomputing combining R and SAGA: The example of landslide susceptibility analysis with generalized additive models, SAGA-Seconds Out, 19, 23–32, 2008. 855

Brenning, A., Gruber, S., and Hoelzle, M.: Sampling and statistical analyses of BTS measurements, Permafr. Periglac. Proc., 16, 383–393, doi:10.1002/ppp.541, 2005. 863

Center, U.: GTOPO30 documentation (README file), Land Processes Distributed Active Archive Center, available online at: http://eros.usgs.gov/Find_Data/Products_and_Data_Available/GTOPO30, 1997. 856

TCD
6, 849–891, 2012

Cohen, J.: A Coefficient of Agreement for Nominal Scales, Educat. Psychol. Meas., 20, 37–46, doi:10.1177/001316446002000104, 1960. 858

Cremonese, E., Gruber, S., Phillips, M., Pogliotti, P., Boeckli, L., Noetzli, J., Suter, C., Bodin, X., Crepaz, A., Kellerer-Pirklbauer, A., Lang, K., Letey, S., Mair, V., Morradi Cella, U., Ravanel, L., Scapozza, C., Seppi, R., and Zischg, A.: Brief Communication: "An inventory of permafrost evidence for the European Alps", The Cryosphere, 5, 651–657, doi:10.5194/tc-5-651-2011, 2011. 858, 861, 863, 884, 885

Delaloye, R., Reynard, E., Lambiel, C., Marescot, L., and Monnet, R.: Thermal anomaly in a cold scree slope (Creux du Van, Switzerland), in: Proceedings of the 8th International Conference on Permafrost. Zurich, Switzerland, 1, 175–180, 2003. 861

Ebohon, B. and Schrott, L.: Modeling mountain permafrost distribution: A new map of Austria, in: Proceedings of the 9th International Conference on Permafrost. Fairbanks, Alaska, 30 June–3 July, 397–402, 2008. 851, 852, 864

Efthymiadis, D., Jones, P., Briffa, K., Auer, I., Böhm, R., Schöner, W., Frei, C., and Schmidli, J.: Construction of a 10-min-gridded precipitation data set for the Greater Alpine Region for 1800–2003, J. Geophys. Res., 110, D01105, doi:10.1029/2005JD006120, 2006. 856

Etzelmüller, B., Farbrot, H., Gudhmundsson, A., Humlum, O., Tveito, O., and Björnsson, H.: The regional distribution of mountain permafrost in Iceland, Permafrost Periglac. Proc., 18, 185–199, doi:10.1002/ppp.583, 2007. 852

Fontana, F., Rixen, C., Jonas, T., Aberegg, G., and Wunderle, S.: Alpine Grassland Phenology as Seen in AVHRR, VEGETATION, and MODIS NDVI Time Series – a Comparison with In Situ Measurements, Sensors, 8, 2833–2853, doi:10.3390/s8042833, 2008. 858

Frauenfelder, R.: Rock glaciers, Fletschhorn Area, Valais, Switzerland, International Permafrost Association, Data and Information Working Group, NSIDC, University of Colorado at Boulder, CO, USA, 1998. 850

Frauenfelder, R., Schneider, B., and Kääb, A.: Using dynamic modelling to simulate the distribution of rockglaciers, Geomorphology, 93, 130–143, doi:10.1016/j.geomorph.2006.12.023, 2008. 860

Gorbunov, A. P., Marchenko, S. S., and Seversky, E. V.: The thermal environment of blocky materials in the mountains of Central Asia, Permafrost Periglac. Proc., 15, 95–98, doi:10.1002/ppp.478, 2004. 861

Gruber, S.: Derivation and analysis of a high-resolution estimate of global permafrost zonation, The Cryosphere, 6, 221–233, doi:10.5194/tc-6-221-2012, 2012. 855

TCD
6, 849–891, 2012

Gruber, S. and Haeberli, W.: Permafrost in steep bedrock slopes and its temperature-related destabilization following climate change, Journal of Geophysical Research, 112, F02S18, doi:10.1029/2006JF000547, 2007. 859, 867

Gruber, S. and Hoelzle, M.: Statistical modelling of mountain permafrost distribution: local calibration and incorporation of remotely sensed data, Permafrost Periglac. Proc., 12, 69–77, doi:10.1002/ppp.374, 2001. 850

Gruber, S. and Hoelzle, M.: The cooling effect of coarse blocks revisited: a modeling study of a purely conductive mechanism, in: Proceedings of the 9th International Conference on Permafrost. Fairbanks, Alaska, 30 June–3 July, 1, 557–561, 2008. 861

Gruber, S., Peter, M., Hoelzle, M., Woodhatch, I., and Haeberli, W.: Surface temperatures in steep Alpine rock faces – a strategy for regional-scale measurement and modelling, in: Proceedings of the 8th International Conference on Permafrost. Zurich, Switzerland, 21–25 July, 1, 325–330, 2003. 859

Gubler, S., Fiddes, J., Keller, M., and Gruber, S.: Scale-dependent measurement and analysis of ground surface temperature variability in alpine terrain, The Cryosphere, 5, 431–443, doi:10.5194/tc-5-431-2011, 2011. 854, 861

Haeberli, W.: Untersuchungen zur Verbreitung von Permafrost zwischen Flüelapass und Piz Grialetsch (Graubünden), Mitteilungen der Versuchsanstalt für Wasserbau, Hydrologie und Glaziologie der ETH Zürich, Zurich, Switzerland, 17, 221 pp., 1975. 861

Haeberli, W. and Funk, M.: Borehole temperatures at the Colle Gnifetti core-drilling site (Monte Rosa, Swiss Alps), J. Glaciol., 37, 37–46, 1991. 862

Haeberli, W., Hallet, B., Arenson, L., Elconin, R., Humlum, O., Kääb, A., Kaufmann, V., Ladanyi, B., Matsuoka, N., Springman, S., and Mühll, D. V.: Permafrost creep and rock glacier dynamics, Permafrost Periglac. Proc., 17, 189–214, doi:10.1002/ppp.561, 2006. 860, 867

Hanson, S. and Hoelzle, M.: Installation of a shallow borehole network and monitoring of the ground thermal regime of a high alpine discontinuous permafrost environment, Eastern Swiss Alps, Norsk Geografisk Tidsskrift – Norwegian J.Geogr., 59, 84–93, doi:10.1080/00291950510020664, 2005. 861

Harris, C., Arenson, L. U., Christiansen, H. H., Etzelmüller, B., Frauenfelder, R., Gruber, S., Haeberli, W., Hauck, C., Hölzle, M., Humlum, O., Isaksen, K., Kääb, A., Kern-Lütschg, M. A., Lehning, M., Matsuoka, N., Murton, J. B., Nötzli, J., Phillips, M., Ross, N., Seppälä, M., Springman, S. M., and Mühll, D. V.: Permafrost and climate in Europe: Monitoring and modelling thermal, geomorphological and geotechnical responses, Earth-Sci. Rev., 92, 117–171,

TCD
6, 849–891, 2012

doi:10.1016/j.earscirev.2008.12.002, 2009. 852
Harris, S. and Pedersen, D.: Thermal regimes beneath coarse blocky materials, Permafrost Periglac. Proc., 9, 107–120, doi:10.1002/(SICI)1099-1530(199804/06)9:2<107::AID-PPP277>3.0.CO;2-G, 1998. 861, 866
Hasler, A., Gruber, S., and Haeberli, W.: Temperature variability and offset in steep alpine rock and ice faces, The Cryosphere, 5, 977–988, doi:10.5194/tc-5-977-2011, 2011. 859, 866
Hayakawa, Y., Oguchi, T., and Lin, Z.: Comparison of new and existing global digital elevation models: ASTER G-DEM and SRTM-3, Geophys. Res. Lett., 35, L17404, doi:10.1029/2008GL035036, 2008. 854
Heggem, E., Juliussen, H., and Etzelmüller, B.: Mountain permafrost in central-eastern Norway, Norsk Geografisk Tidsskrift – Norweg. J. Geogr., 59, 94–108, doi:10.1080/00291950510038377, 2005. 852
Heginbottom, J.: Permafrost mapping: a review, Prog. Phys. Geogr., 26, 623–642, doi:10.1191/0309133302pp355ra, 2002. 852
Hiebl, J., Auer, I., Böhm, R., Schöner, W., Maugeri, M., Lentini, G., Spinoni, J., Brunetti, M., Nanni, T., Perčec Tadić, M., Bihari, Z., Dolinar, M., and Müller-Westermeier, G.: A high-resolution 1961–1990 monthly temperature climatology for the greater Alpine region, Meteorol. Zeitschr., 18, 507–530, doi:10.1127/0941-2948/2009/0403, 2009. 856
Hijmans, R. J. and van Etten, J.: raster: Geographic analysis and modeling with raster data, R package version 1.9-64, The R Foundation for Statistical Computing, Vienna, Austria, 2012. 855
Hoelzle, M.: Permafrost occurrence from BTS measurements and climatic parameters in the Eastern Swiss Alps, Permafrost Periglac. Proc., 3, 143–147, doi:10.1002/ppp.3430030212, 1992. 852
Hoelzle, M.: Permafrost und Gletscher im Oberengadin: Grundlagen und Anwendungsbeispiele für automatisierte Schätzverfahren, Mitteilungen der VAW-ETH Zurich, 132, 121 pp., 1994. 850
Hoelzle, M., Haeberli, W., and Keller, F.: Application of BTS-measurements for modelling permafrost distribution in the Swiss Alps, in: Proceedings of the 6th International Conference on Permafrost, South China University Technology Press, Beijing, China, 272–277, 1993. 852, 861
Hoelzle, M., Haeberli, W., and Stocker-Mittaz, C.: Miniature ground temperature data logger measurements 2000–2002 in the Murtèl-Corvatsch area, Eastern Swiss Alps, in: Proceed-

TCD
6, 849–891, 2012

ings of the 8th International Conference on Permafrost. Zurich, Switzerland, 21–25 July, 419–424, 2003. 863
Hosmer, D. and Lemeshow, S.: Applied logistic regression, Wiley-Interscience, New York, USA, 2000. 863
Huete, A.: A soil-adjusted vegetation index (SAVI), Remote Sensing of Environment, 25, 295–309, doi:10.1016/0034-4257(88)90106-X, 1988. 857, 858
Humlum, O.: Active layer thermal regime at three rock glaciers in Greenland, Permafrost Periglac. Proc., 8, 383–408, doi:10.1002/(SICI)1099-1530(199710/12)8:4<383::AID-PPP265>3.0.CO;2-V, 1997. 861
Imhof, M.: Modelling and verification of the permafrost distribution in the Bernese Alps, Switzerland, Permafrost Periglac. Proc., 17, 267–280, doi:10.1002/(SICI)1099-1530(199609)7:3<267::AID-PPP221>3.0.CO;2-L, 1996. 850, 852
International Organization for Standardization: International Standard Atmosphere, Standard Atmosphere, ISO 2533:1975, 1975. 856
Janke, J. R.: The occurrence of alpine permafrost in the Front Range of Colorado, Geomorphology, 67, 375–389, doi:10.1016/j.geomorph.2004.11.005, 2004. 852
Juliussen, H. and Humlum, O.: Thermal regime of openwork block fields on the mountains Elgåhogna and Sølen, central-eastern Norway, Permafrost Periglac. Proc., 19, 1–18, doi:10.1002/ppp.607, 2008. 861, 866
Keller, F.: Automated mapping of mountain permafrost using the program PERMAKART within the geographical information system ARC/INFO, Permafrost Periglac. Proc., 3, 133–138, doi:10.1002/ppp.3430030210, 1992. 852
Keller, F., Frauenfelder, R., Hoelzle, M., Kneisel, C., Lugon, R., Phillips, M., Reynard, E., and Wenker, L.: Permafrost map of Switzerland, in: Proceedings of the 7th International Conference on Permafrost. Nordicana, Yellowknife, Canada, 23–27 June, 557–562, 1998. 850, 864
Kneisel, C.: New insights into mountain permafrost occurrence and characteristics in glacier forefields at high altitude through the application of 2D resistivity imaging, Permafrost Periglac. Proc., 15, 221–227, doi:10.1002/ppp.495, 2004. 867
Kneisel, C. and Kääb, A.: Mountain permafrost dynamics within a recently exposed glacier forefield inferred by a combined geomorphological, geophysical and photogrammetrical approach, Earth Surf. Process. Landf., 32, 1797–1810, doi:10.1002/esp.1488, 2007. 867

TCD
6, 849–891, 2012

Kneisel, C., Haeberli, W., and Baumhauer, R.: Comparison of spatial modelling and field evidence of glacier/permafrost relations in an Alpine permafrost environment, Ann. Glaciol., 31, 269–274, 2000. 862
Lambiel, C. and Reynard, E.: Regional modelling of present, past and future potential distribution of discontinuous permafrost based on a rock glacier inventory in the Bagnes-Heé reé mence area (Western Swiss Alps), Norsk Geografisk Tidsskrift – Norweg. J. Geogr., 55, 219–223, 2001. 850
Lewkowicz, A. and Bonnaventure, P.: Interchangeability of mountain permafrost probability models, northwest Canada, Permafrost Periglac. Process., 19, 49–62, doi:10.1002/ppp.612, 2008. 852
Lewkowicz, A. G. and Ednie, M.: Probability mapping of mountain permafrost using the BTS method, Wolf Creek, Yukon Territory, Canada, Permafrost Periglac. Process, 15, 67–80, doi:10.1002/ppp.480, 2004. 852
Li, J., Sheng, Y., Wu, J., Chen, J., and Zhang, X.: Probability distribution of permafrost along a transportation corridor in the northeastern Qinghai province of China, Cold Reg. Sci. Technol., 59, 12–18, doi:10.1016/j.coldregions.2009.05.012, 2009. 852
Mason, S. and Graham, N.: Areas beneath the relative operating characteristics (roc) and relative operating levels (rol) curves: Statistical significance and interpretation, Q. J. Roy. Meteorol. Soc., 128, 2145–2166, doi:10.1256/003590002320603584, 2002. 855
Matsuoka, N., Ikeda, A., and Date, T.: Morphometric analysis of solifluction lobes and rock glaciers in the Swiss Alps, Permafrost Periglac. Process., 16, 99–113, doi:10.1002/ppp.517, 2005. 866
Noetzli, J. and Gruber, S.: Transient thermal effects in Alpine permafrost, The Cryosphere, 3, 85–99, doi:10.5194/tc-3-85-2009, 2009. 867
Paul, F., Frey, H., and Le Bris, R.: A new glacier inventory for the European Alps from Landsat TM scenes of 2003: Challenges and results, Ann. Glaciol., 52, 144–152, 2011. 858
PERMAFRANCE: Permafrost in France, edited by: Schoeneich, P,. Bodin, X., Krysiecki, J. M., Deline, P. and Ravanels, L., Permafrance Network, Report Nr. 1, 68 pp., 2010. 865
Pogliotti, P.: Influence of snow cover on MAGST over complex morphologies in mountain permafrost regions, Ph.D. thesis, Earth Science Department, University of Turin, Italy, 2010. 857, 859
R Development Core Team: Development Core Team: R: a language and environment for statistical computing, R Foundation for Statistical Computing, Vienna, Austria, ISBN 3-900051-

TCD
6, 849–891, 2012

07-0, available online at: http://www.R-project.org, 2010. 855
Serrano, E., Agudo, C., Delaloye, R., and Gonzalez-Trueba, J.: Permafrost distribution in the Posets massif, Central Pyrenees, Norsk Geografisk Tidsskrift – Norw. J. Geogr., 55, 245–252, 2001. 852
swisstopo: Vector 25 - das digitale Landschaftsmodell der Schweiz, Bundesamt für Landestopographie, Wabern, Switzerland, 2007. 857
Tanarro, L., Hoelzle, M., García, A., Ramos, M., Gruber, S., Gómez, A., Piquer, M., and Palacios, D.: Permafrost distribution modelling in the mountains of the Mediterranean: Corral del Veleta, Sierra Nevada, Spain, Norsk Geografisk Tidsskrift – Norweg. J. Geogr., 55, 253–260, 2001. 852
Travis, M. R., Elsner, G. H., Iverson, W. D., and Johnson, C. G.: VIEWIT: computation of seen areas, slope, and aspect for land-use planning, PSW 11/1975, Pacific Southwest Forest and Range Experimental Station, Berkley, California, USA, 1975. 856
Vincent, C., Le Meur, E., Six, D., Possenti, P., Lefebvre, E., and Funk, M.: Climate warming revealed by englacial temperatures at Col du Dôme (4250 m, Mont Blanc area), Geophys. Res. Lett., 34, 16502, doi:10.1029/2007GL029933, 2007. 862
Zhang, T., Heginbottom, J. A., Barry, R. G., and Brown, J.: Further statistics on the distribution of permafrost and ground ice in the Northern Hemisphere, Polar Geogr., 24, 126–131, doi:10.1080/10889370009377692, 2000. 855

TCD
6, 849–891, 2012

Table 1. Overview of Landsat scenes used to calculate the SAVI index.

Path	Row	Date (d/m/y)	Sensor
191	27	14/10/2006	Landsat 5
191	28	14/10/2006	Landsat 5
192	27	05/10/2006	Landsat 5
192	28	22/08/2007	Landsat 5
193	27	20/10/2003	Landsat 5
193	28	34/08/2003	Landsat 5
194	27	21/08/2000	Landsat 7
194	28	32/10/2002	Landsat 7
195	27	24/08/2006	Landsat 5
195	28	18/10/2003	Landsat 5
195	29	06/09/2002	Landsat 7
196	28	23/08/2003	Landsat 5
196	29	23/08/2003	Landsat 5

TCD
6, 849–891, 2012

Table 2. Thresholds and corresponding weights per variable that were used to characterize the agreement of the terrain attributes (PF_{loc}) for the evaluation data. The weight for the variable aspect was fixed for slope angles ≤ 15° (derived from ASTER GDEM) to 2, because uncertainties in this variable are large for flat terrain.

Weights	Elevation [m]	Slope angle [°]	Aspect [°][a]
2	< 100	< 10	< 25
1	100–250	10–25	25–50
0	> 250	> 25	> 50

[a] Only applied to observations with a slope angle > 15°.

TCD
6, 849–891, 2012

Table 3. Overview of the different observation types (BH: borehole, GST: ground surface temperature, SC: rock fall scar, TR: trench and construction site, SM: surface movement, GP: geophysical investigation, OIE: other indirect evidence) that remain for evaluation. For each type, the number of permafrost-existence (PF_{yes}) and permafrost-absence (PF_{no}) observation is given (Certainty levels PF_{cert}: 1 definite proof, 2 quite certain, 3 quite likely; Agreement levels PF_{loc}: a agree, d disagree, s strongly disagree).

Type	PF_{yes}	PF_{cert} (1/2/3)	PF_{loc} (a/d/s)	PF_{no}	PF_{cert} (1/2/3)	PF_{loc} (a/d/s)
BH	45	36/6/3	22/3/20	16	11/5/0	11/1/4
GST	49	18/25/6	37/3/9	41	3/16/22	34/1/6
SC	36	6/30/0	3/1/32	–	–	–
TR	38	25/12/1	22/0/16	9	3/6/0	6/2/1
SM	4	2/2/0	3/ 0/1	–	–	–
GP	70	29/35/6	61/4/5	11	3/8/0	11/0/0
OIE	33	7/19/7	23/4/6	–	–	–

TCD
6, 849–891, 2012

Table 4. Temperature offsets (°C) that were applied to the different surface types. A positive sign means a positive temperature offset is applied, which results in a more pessimistic permafrost estimate. A negative sign means a more optimistic permafrost estimate.

Surface cover	Δ_R	Δ_{Da}	Δ_{Db}	total offset
Steep bedrock	[−0.5, −2.5]	–	–	[−0.5, −2.5]
Debris cover	–	0.5	–	0.5
Vegetation	–	0.5	2	2.5

TCD
6, 849–891, 2012

Table 5. Estimated permafrost index areas for the entire Alps. The relative area refers to the total area of the Alps (ca. 200 000 km^2).

Permafrost index	Total area [km^2]	Relative area [%]
≥ 0.1	11 627	6
≥ 0.5	6220	3
≥ 0.9	2007	1
Glaciers	2056	1

TCD
6, 849–891, 2012

Table 6. Estimated permafrost index areas for the Alps calculated without the offset Δ_{Db} = 2°C for vegetated areas. ΔA refers to the difference in area between estimated permafrost distribution calculated with (Table 5) and without offset Δ_{Db}.

Permafrost index	Total area [km^2]	ΔA [km^2]
≥ 0.1	14 774	3147
≥ 0.5	6566	346
≥ 0.9	2011	4

TCD
6, 849–891, 2012

Table 7. Estimated permafrost index areas [km^2] for different Alpine countries using different index values, and comparison to glacier area (CH: Switzerland, IT: Italy, AT: Austria, FR: France, DE: Germany, SLO: Slovenia, FL: Liechtenstein).

Country	Index ≥ 0.1	Index ≥ 0.5	Index ≥ 0.9	Glaciers
CH	3710	2163	754	1010
IT	3353	1786	569	441
AT	2907	1557	484	340
FR	1587	703	199	265
DE	44.1	7.6	0.8	0.6
SLO	25.7	3.6	0.1	0.0
FL	0.3	0.0	0.0	0.0
Total	11 626	6220	2007	2056

TCD
6, 849–891, 2012

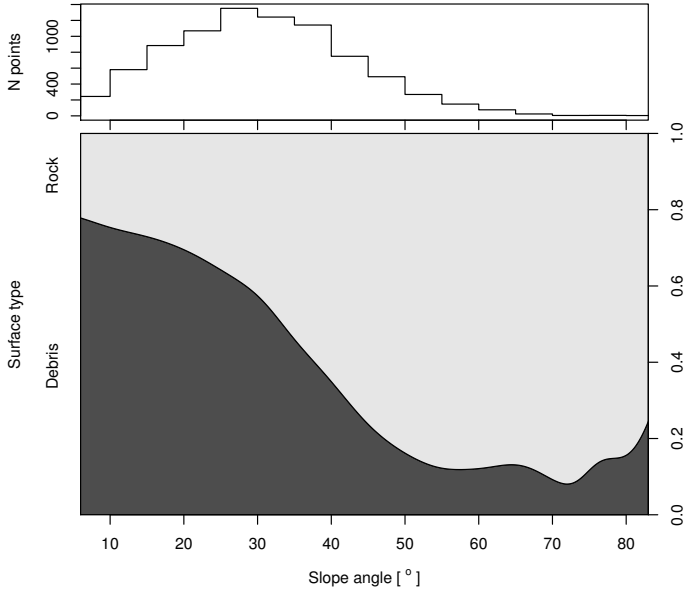

Fig. 1. Conditional density plot for the two surface classes debris and rock (derived from Vector25) in relation to slope angle. Above, the number of points that are used for this analysis are shown in relation to slope angle.

TCD
6, 849–891, 2012

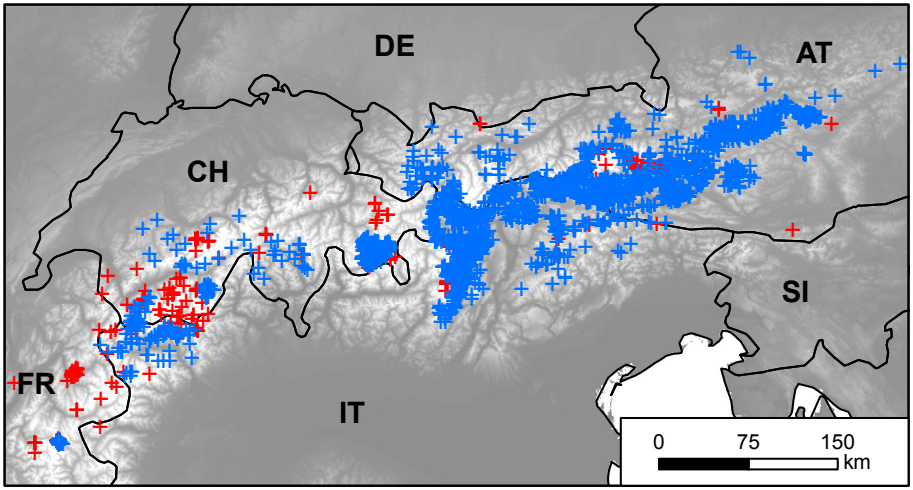

Fig. 2. Spatial distribution of permafrost evidence data (Cremonese et al., 2011), which was not used for model calibration in Boeckli et al. (2012) and is thus available for evaluation. Blue dots represent rock glaciers and red crosses represent point evidences (summarized in Table 3).

TCD
6, 849–891, 2012

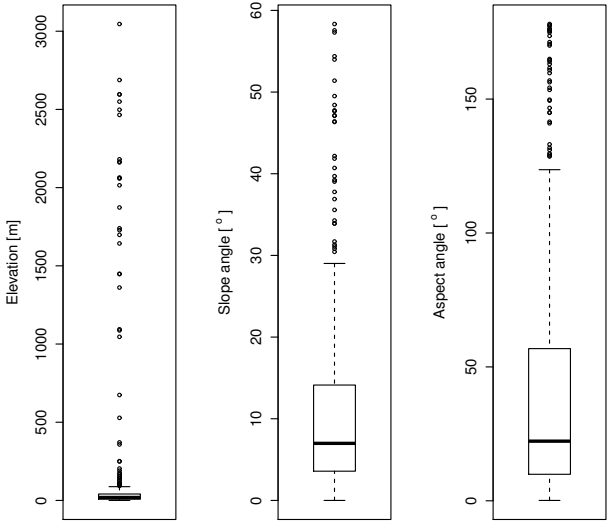

Fig. 3. Absolute difference between terrain variables calculated based on ASTER GDEM and the one provided by the data contributor into the permafrost evidence collection (Cremonese et al., 2011).

TCD
6, 849–891, 2012

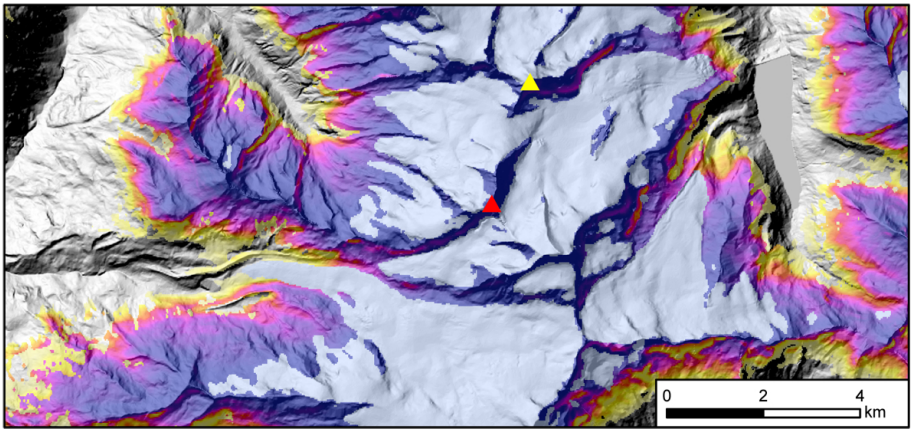

Fig. 4. Alpine Permafrost Index Map (APIM) shown for the area surrounding Rimpfischhorn (4199 m, red triangle) and Allalinhorn (4027 m, yellow triangle) in Switzerland. The map should be interpreted together with the legend and interpretation key (Fig. A1).

TCD
6, 849–891, 2012

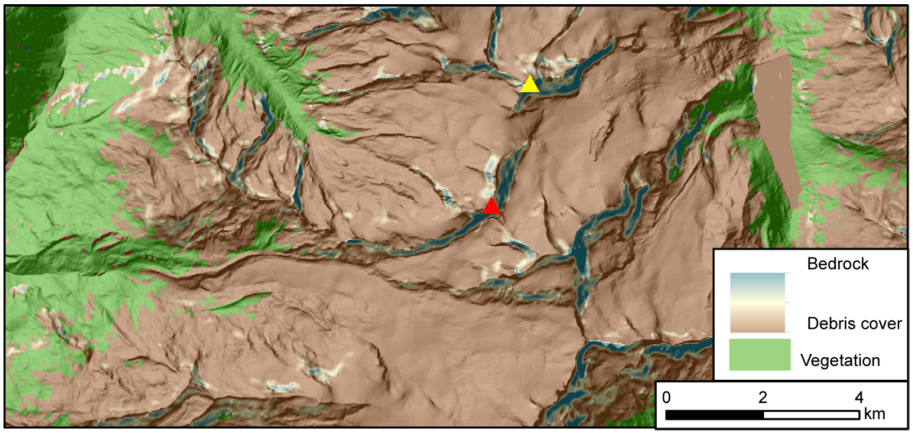

Fig. 5. Surface cover map showing the vegetation mask and the surface class index m_r (Eq. 2) for the same area as Fig. 4. To grid cells with a slope angle $\leq 35^{\circ}$ the debris model, for slope angles $\geq 55^{\circ}$ the rock model is used. In between, a fuzzy membership (linear function depending on slope angle) is applied in order to provide a complete spatial coverage of APIM.

TCD
6, 849–891, 2012

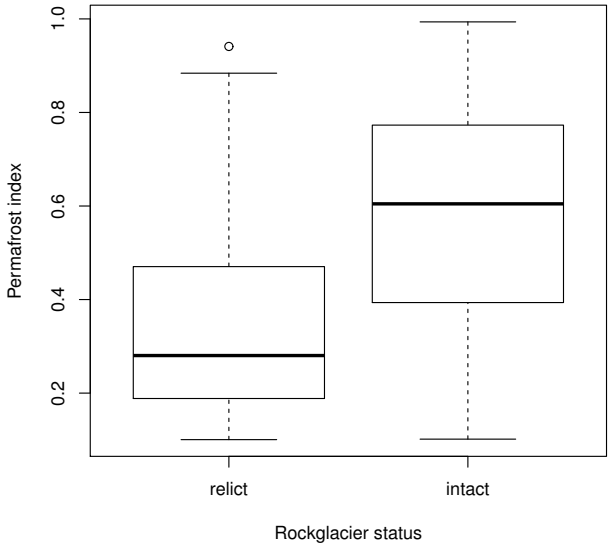

Fig. 6. Permafrost index values for intact and relict rock glaciers that were not used for model calibration. A random point within each rock glacier polygon was used for this figure.

TCD
6, 849–891, 2012

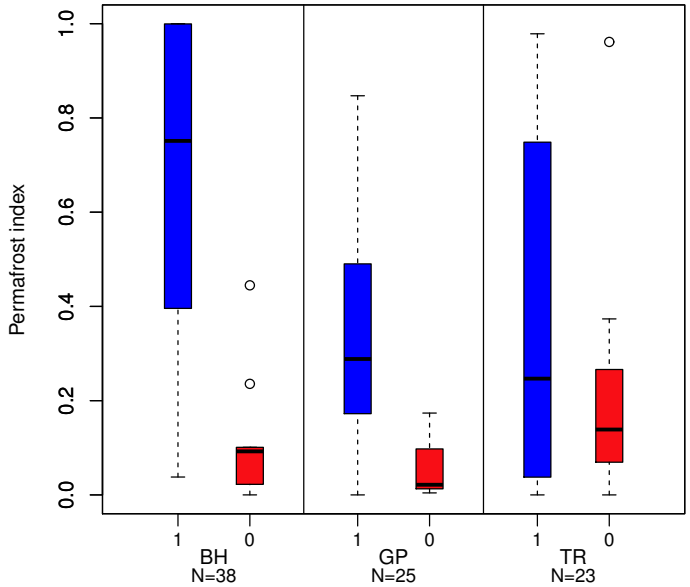

Fig. 7. Box-plots showing predicted permafrost index values for the evidence types "Borehole temperatures" (BH), "Geophysical investigations" (GP) and "Trench or construction sites" (TR) for permafrost-existence (1) and permafrost-absence observations (0).

TCD
6, 849–891, 2012

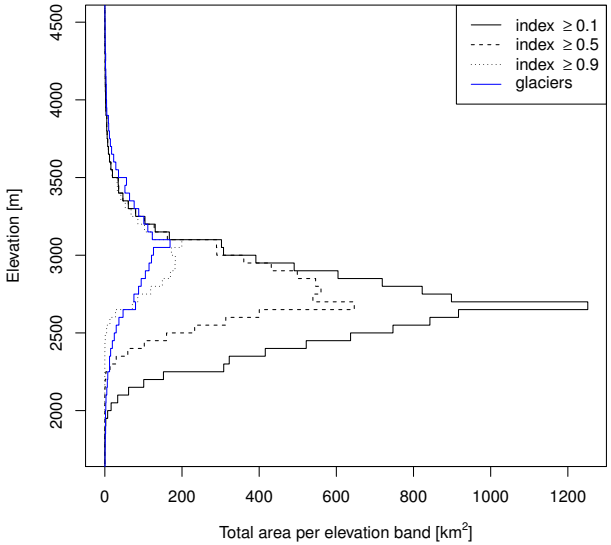

Fig. 8. Altitudinal distribution of permafrost index areas in the Alps, calculated for elevation bands of 50 meters.

TCD
6, 849–891, 2012

TCD
6, 849–891, 2012

Alpine Permafrost Map: Legend, Interpretation Key and Auxiliary Information

Map Legend
This map shows a qualitative index describing how likely permafrost exists. It is consistent for the entire Alps and intended for practical use for infrastructure planning and maintenance.

Blue: Permafrost in nearly all conditions

Purple: Permafrost mostly in cold conditions

Yellow: Permafrost only in very cold conditions

Glacier

Some important local factors such as sub-surface material or snow conditions are not or only approximatively accounted for in the map. However, they can cause strong differences in ground temperature in otherwise equal topograhic situations. For this reason, the map legend is accompanied by the interpretation key, shown on the right, that can be used to locally further refine the estimate shown on the map. As an example, one would not expect permafrost in fine material (B) or in homogeneous rock (H) where a yellow signature is shown on the map. In special circumstances, permafrost can exist outside the area of the color signature shown. The map shows estimated conditions; more certainty can locally be achieved by e.g., geophysics or boreholes.

Auxiliary Information
An additional map shows the surface types that were used. This allows comprehending the applied models (debris and rock model) and offset terms. To grid cells with a slope angle ≤ 35° only the debris model is applied, for slope angles ≥ 55° the rock model is used. In between, a fuzzy membership function is calculated.

1: Steep Bedrock (slope angle ≥ 55°)
0: Debris Cover (slope angle ≤ 35°)
2: Vegetation

Interpretation Key

Clast size, soil properties and vegetation
A cover of coarse blocks with open voids and no infill of fine material (A) indicates cold conditions. Bedrock, fine-grained soil or soil with coarse blocks but an infill of fines (B) indicate warm conditions. A dense vegetation cover (C) usually indicates the absence of permafrost.

Rock glaciers
Active (intact) rock glaciers (D) are identified by signs of movement such as steep fronts. They are reliable visual indicators of permafrost within their creeping mass of debris but do not allow easy conclusions on adjacent areas.

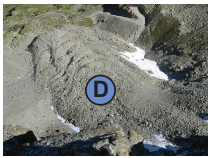

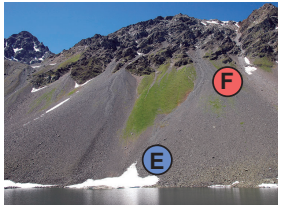

Slope position and long-lasting snow-patches
The position along a slope can affect ground temperatures through the sorting of clasts, air circulation within the slope, and snow re-distribution. Often, the foot of slope (E) has colder ground temperatures. It contains more coarse material and is affected by long-lasting avalanche snow. Similarly, other late-lying snow patches indicate locally cold conditions. The top of slope (F) often has locally rather warm conditions. Frequently, it contains smaller clasts as well as an infill of fine material.

Steep rock slopes
Steep rock slopes have differing degrees of heterogeneity caused by micro-topography and fracturing. Higher heterogeneity (G) often enables a thin snow cover as well as ventilation and deposition of snow in large fractures, indicating locally cold conditions. Steep, smooth and largely unfractured rock (H) is indicative of warmer conditions. This effect is more pronounced in sun-exposed than in shaded locations.

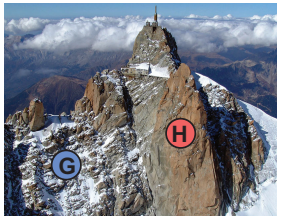

Fig. A1. Legend, interpretation key and auxiliary information that is provided with the Alpine Permafrost Index Map (APIM). This information helps to assess map uncertainties, to relate map contents to their actual expression in terrain and to comprehend the applied models and offset terms.